LRP 584/97 August 1997

Invited Papers
Presented at the

36TH IEEE CONFERENCE ON
DECISION AND CONTROL

SAN DIEGO, CALIFORNIA, USA
10-12 DECEMBER 1997

Table of Contents

CAN BETTER MODELLING IMPROVE TOKAMAK CONTROL?

J.B. Lister (jo.lister@epfl.ch), P. Vyas, D.J. Ward

Centre de Recherches en Physique des Plasmas, Association EURATOM-Confédération Suisse, Ecole Polytechnique Fédérale de Lausanne, Lausanne, Switzerland

R. Albanese, G. Ambrosino, M. Ariola, F. Villone

Consorzio CREATE, Associazione EURATOM/ENEA/CREATE, c/o Dipartimento di Ingegneria Elettrica, Università "Federico II" di Napoli, Naples, Italy

A. Coutlis, D.J.N. Limebeer, J.P. Wainwright

Centre for Process Systems Engineering, Imperial College of Science, Technology and Medicine, London, United Kingdom

ABSTRACT

The control of present day tokamaks usually relies upon primitive modelling and TCV is used to illustrate this. A counter example is provided by the successful implementation of high order SISO controllers on COMPASS-D. Suitable models of tokamaks are required to exploit the potential of modern control techniques. A physics based MIMO model of TCV is presented and validated with experimental closed loop responses. A system identified open loop model is also presented. An enhanced controller based on these models is designed and the performance improvements discussed.

1. INTRODUCTION

Tokamaks are devices in which a plasma is magnetically confined and have the potential to form the basis of future nuclear fusion power plants. A tokamak fusion reactor would require the plasma to maintain a temperature of over 10^{8}°C and a current of order 10^{7}A. Such reactors could offer very significant environmental advantages over existing power plants.

Many control problems feature significantly in the operation of tokamaks, including the control of the plasma density and plasma heating. Most control design effort is concerned with the electromagnetic control of the plasma current, shape and position. In this case the actuators are a set of "poloidal field" coils distributed around the vacuum vessel. Voltages are applied to these coils driving coil currents which produce magnetic fields. The field interacts with the plasma to change its shape and position and to induce plasma current.

As an illustration, Fig. 1 shows the TCV tokamak which is ideally suited to control studies. There are over 76 magnetic flux/field sensors which are combined to generate five control variables, one representing the plasma current, two representing the plasma vertical and horizontal position, and two more representing the shape of the plasma. There are 18 independently powered poloidal field coil sets.

The design of control systems for the electromagnetic system is usually based on primitive models of the plasma. The most important property of the models is the instability of the vertical position in plasmas which are elongated in the vertical direction. Multivariable models are often used because of the high degree of coupling between control variables. The presence of the vacuum vessel surrounding the plasma is critical, since image currents are induced in this conducting structure whenever the magnetic flux varies. However, the design of the controllers usually neglects the presence of these image currents, except for the control of the vertical position.

Although the present degree of control is satisfactory, it is likely that improvements are possible if more detailed tokamak models are considered. Improvements could be made to stabilize plasmas with higher instability growth rates, improve disturbance and noise rejection, improve the decoupling of control variables when tracking reference changes and to reduce the power requirements of the poloidal field coil system. These improvements are useful for current experiments, but most importantly are motivated by the more stringent requirements of the control of ITER plasmas, described in detail in companion papers.

Improved models can be used to optimize the performance of a tokamak either by allowing fine-tuning of existing controllers or by using optimal control theory. One of the advantages of the simple controllers used at present is their robust stability. This is a necessity given the crude approximations made in the underlying models. The question remains open whether highly tuned, high performance controllers will have suitable robust stability properties.

The structure of the present paper is as follows. In Section 2 we investigate a SISO system from the COMPASS-D tokamak, in which a high level of power

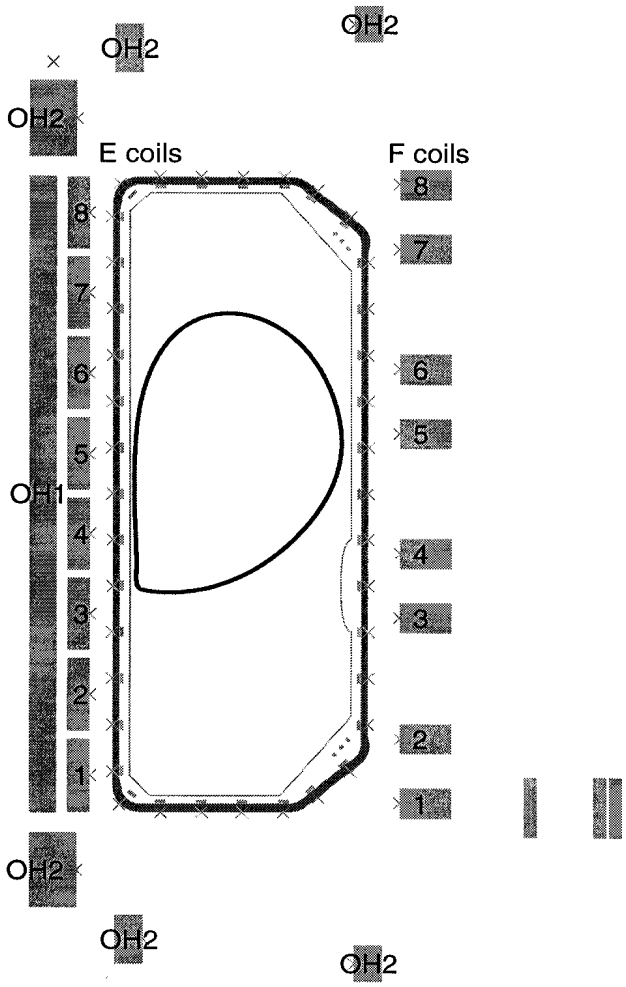

Figure 1. The TCV tokamak, with the vacuum vessel, poloidal field coils (E/F1 to E/F8, OH1 and OH2), poloidal field probes (marked '-' inside graphite tiles) and flux loops (marked 'x' on the vacuum vessel). The plasma boundary of a single-null diverted plasma is shown inside the vessel.

supply noise is encountered in the vertical position loop when using a P+D controller. The performance benefits demonstrated on COMPASS-D provide strong motivation for investigating modelling and control of other control loops. This has been performed on the TCV tokamak where two approaches have been made at establishing a MIMO model. In Section 3 we describe the essential features of the TCV electromagnetic control system. The closed loop behaviour of a MIMO linearized phenomenological model of TCV is compared with experimental results in Section 4. Although the results of these closed loop comparisons appear excellent, this does not necessarily imply that the underlying open loop models are adequate for the design of a controller. Section 5 describes closed loop system identification experiments designed to identify the open loop plant model. The identified and physics models are compared.

In Section 6 we summarize the present relatively simple control of TCV plasmas, indicating both its strengths and its weaknesses, and present results from a high order controller. Section 7 draws conclusions from this work.

2. VERTICAL POSITION ON COMPASS-D

In experiments on the COMPASS-D tokamak, the vertical position control signal is dominated by a 600Hz component, and higher harmonics [1]. This is due to interference from 12 phase thyristor rectifiers used in radial position, shape, and plasma current control loops. Velocity measurements inside the vessel also have a much larger high frequency (above 3kHz) noise component than the external measurements.

An analogue P+D controller is used to regulate the plasma vertical position. Sensor coils inside the vessel are used for the derivative part of the control signal and the proportional component is obtained by integrating the velocity signals from coils outside the vessel. The resulting system can be tuned to provide an adequate degree of stability.

Antiparallel coils above and below the plasma generate a radial field controlling the vertical position. These are driven by a high bandwidth linear transistor amplifier. The shape and position loops are effectively decoupled from each other since the shaping field is preprogrammed and constant throughout a discharge. The radial position is stable with relatively slow dynamics and the vertical position is unstable on relatively fast timescales, with a growth rate of $2500s^{-1}$. The vertical and radial field coils are chosen to minimize coupling so the vertical stability problem can be considered independently of the other parameters.

System identification was used to obtain a model of the open loop plasma vertical position response to control coil currents, directly from COMPASS–D experimental data. The response depends strongly on plasma properties, such as the shape, and models based on plasmas with different elongations and triangularities have been identified.

Since the plant is unstable, the system had to be identified in closed loop. A persistently exciting reference input signal was created using a Random Binary Sequence (RBS) to perturb the plasma vertical position. The resulting control coil currents and position signals were sampled and then filtered to remove a 600Hz noise component and low frequency drift. Mathematical fits of the parameters of models to the resulting experimental data were made.

Two types of model structure were identified. The first is the ARX model where the parameters were found from a least squares fit and the residuals represent noise in the system. For COMPASS-D many different model orders were tested and the simplest model order with reasonable residual costs was found. More complicated models provided no significant improvement in the residual cost. The transfer functions of the resulting models have a single unstable pole.

The second model structure was a bicausal FIR model which is simply the impulse response of the open loop system. A causal part of the FIR represents the stable part of the plant and a noncausal part represents the plant instability. The coefficients were found from a least squares fit to the experimental data. The frequency response functions of both the ARX and FIR models were

similar and within confidence bounds derived from the residuals.

The instability growth rate increases if the shaping field is increased, consistent with physical models. The bandwidth of the frequency response increases and the DC gain decreases with increasing shape. The phase lead of the model also decreases with shape. The effect of the shielding by the vessel wall is observed when comparing models derived from external or internal coils. The amplitude response of the external coil model has a faster roll–off and there is less phase lead than in the internal coil model.

Having developed the system identification technique, two sets of model comparisons were made. Firstly we compared the instability growth rates from the identified ARX model to growth rates obtained from the PACE rigid current displacement model. This was done for plasmas with different shapes and correspondingly different instability growth rates. The agreement between the two models was found to be good.

A second assessment of the ARX and FIR models was to compare predictions of upper and lower gain margins, and the corresponding phase crossover frequencies, with experimental values. The stability margins were determined experimentally by deliberately changing the loop gain until loss of control occurred. Predictions of closed loop gain stability margins and frequencies and experimentally determined values were found to be in good agreement. It was found that the P and D gains in use, chosen empirically without a model, were optimal in the sense of providing a critically damped response.

The use of internal measurements in the COMPASS–D P+D control loop results in a large stability margin, i.e., relatively large changes in the frequency response can occur without the system becoming unstable. The 600Hz noise on COMPASS–D could have been reduced by adding a notch filter to the P+D controller, but this would lead to more phase lag below 600Hz and would reduce the stability margins.

High order controllers designed using modern control theory were developed and were tested on COMPASS–D [2,3]. The controllers were developed using the system identified ARX model and were implemented on a Digital Signal Processor (DSP). Two types of controller were developed, one designed in the continuous time domain using $\mathbf{H}_\infty$ control theory, and another designed in discrete time using the SGPC (Stable Generalised Predictive Control) technique. The $\mathbf{H}_\infty$ controller was designed by specifying maximum bounds on the maximum magnitudes of various closed loop frequency responses, and the optimal controller maximising a measure of stability margin was calculated. The bounds were used to constrain to a very small value the closed loop gain at 600Hz, in order to attenuate the noise. Another constraint was used at high frequency to limit the controller response to high frequency noise. Another bound was used to ensure that the steady state error between the reference position signal and measured closed loop response was small. The resulting

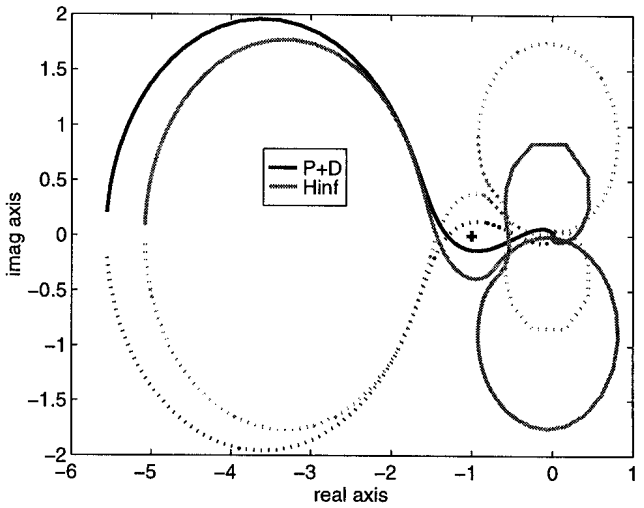

Figure 2. Nyquist plot of COMPASS-D vertical position loop with P+D and $\mathbf{H}_\infty$ controllers.

continuous time controller was converted to discrete time using the Tustin bilinear approximation before implementation on the DSP.

The SGPC controller was designed in two stages by separating the performance and the robust stability criteria. The plant model was modified to include a 600Hz notch filter and then a controller minimizing a time domain cost function was calculated. The cost was the weighted sum of the squares of the closed loop position error and control signal changes to a step input over a finite receding horizon. The second stage was then to maximize the robust stability margin of the system which was defined in the frequency domain in a similar manner to that used in the $\mathbf{H}_\infty$ controller. The controller was structured in a way such that changing the robust stability margin did not affect the performance cost. A large 600Hz penalty was used in the stability margin constraint to maintain the noise rejection properties of the notch filter.

The Nyquist plots of the P+D and $\mathbf{H}_\infty$ controllers are shown in Figure 2. Since the plant has one unstable pole, the Nyquist plot should encircle the -1+0j point once anticlockwise for closed loop stability. The P+D loop passes relatively close to the -1+0j point indicating a poor stability margin. Although in theory the system is stable, in experiments the system is unstable providing evidence of a small degree of modelling error. The extra degrees of freedom offered by the high order $\mathbf{H}_\infty$ controller can be used to improve the stability margin, despite the notch in gain at 600Hz which is the frequency at which the plot passes close to the origin.

Experimental results showed that both high order controllers stabilized the plasma with only external measurements and reduce the effects of 600Hz noise on the control signal. Neither of these attributes are possible with a simple P+D controller. An important factor in the success of the controllers was the characterization of the various sources of noise and disturbances in the system and the estimation of the accuracy of the model. Large high frequency gains in controllers can produce large stability margins but can also contribute to the

amplification of high frequency noise in the system. The trade-off between the two effects needs to be selected carefully. This was found to be as equally important as the dynamical model itself in producing a controller of utility in an experiment rather than a simulation.

3. TCV MODELLING

Given the success of the SISO high order controllers on COMPASS-D and the theoretical benefits of high order MIMO controllers for ITER, it was decided to undertake a program of MIMO modelling and control on the TCV tokamak. Two different modelling approaches were investigated with the aim of qualifying their use for controller design and eventually testing the potential benefits offered by improved controllers. One approach uses a phenomenological model and the other uses system identification to develop the model. Both were validated on TCV with the present TCV PCG control system [4].

The model inputs consist of the voltages applied to the 18 poloidal field coils (Fig. 1) and the outputs are the 5 control variables, namely the plasma current, the plasma vertical position, the horizontal position and the two shape variables which are the curvature of the magnetic field on the inboard and outboard sides of the tokamak respectively. These control variables are constructed from linear combinations of 38 poloidal flux, 38 poloidal field and 18 poloidal field coil current measurements

Each poloidal field coil is powered by a 12-phase thyristor AC-DC converter (PS), which introduces both a ripple due to the thyristor firing and a delay due to the switching times at which the thyristors are fired. Such a supply is highly nonlinear but was approximated as a linear system. We chose to model the PS using only a single pole filter, approximating the time delay and bandwidth of the PS. The magnitude of the pole was tuned to match observations. It is important to emphasize that at no time were the models "tuned" to enhance the agreement in the results which were obtained.

4. CREATE-L PHYSICS MODEL

Many plasma models are currently being used during the ITER design and their physics assumptions differ considerably. It was considered essential to validate one of these models extensively on an existing tokamak. We have chosen the CREATE-L model [5], referred to in a companion paper, since it is widely used by the European Home Team in the ITER design and since it is relatively simple while remaining based on a physical model of the plasma equilibrium. It is a linearized model, allowing its straightforward use in the design and testing of feedback controllers in simulations.

The full CREATE-L model of the linearized response of a TCV plasma can be considered as containing three basic components. The first component describes the general response of a plasma to changes in the currents in the passive structures of the vessel or currents in the poloidal field coils. The second component essentially quantifies the vacuum properties of the active poloidal field coils and passive structures of the tokamak, including their

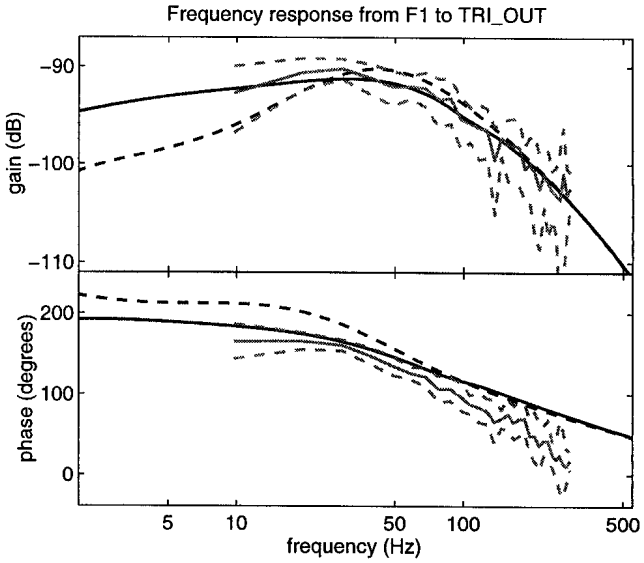

Figure 3. Experimental and modelled frequency responses of outboard field curvature (TRI_OUT) to stimulation from coil F1. Experimental response (light solid) with confidence bounds (light dashed), CREATE-L (dark solid), plasmaless (dark dashed).

physical location, their resistances and their mutual inductances. The state equation model order is 75. The third component comprises the modelling of the sensor signals used as inputs to the TCV control loop and the properties of the feedback controller and includes the power supplies.

As described in detail elsewhere [5] the determining equations can be converted to standard state space form. The linearized model predicts linearized output parameters such as field or flux measurements, separatrix gap deviations or velocities for diverted plasmas.

Two different plasma shapes were validated against their corresponding model. A "limited" plasma [6] which was up-down symmetric and where the plasma vertical and horizontal responses are not coupled was first compared. This was followed by a "diverted" up-down asymmetric plasma [7] where the horizontal and vertical positions were now coupled.

Test signals were applied to the various combinations of poloidal field coils to excite a wide range of responses. The resulting closed loop responses of the control variables on TCV were compared to simulated responses. Square pulse stimulation signals were used to make the model-experiment comparisons in the time domain. Quantities such as the low frequency gain, the overshoot and the rise time of the responses are easily judged by eye. Excitation of the same coil combinations using an RBS signal does not lend itself to a simple visual comparison, but it provides a very rich excitation over a wide range of frequencies. This allowed a subsequent comparison of the frequency domain response, a typical example being Fig. 3.

When comparing the experimental results with the predictions of the model, we questioned the importance of the plasma model itself to the accuracy of the simulations. Control variables not related to a plasma current moment

can be fairly well approximated with a plasmaless model. However the use of the extensive coil set on TCV produced widely varying responses. The closed loop simulations proved to be sensitive to the model plasma shape and some of the model physics assumptions.

The overall agreement between the model and the experimental data is good for both the time and frequency domains and the limited and diverted plasmas. There is no evidence to suggest that the CREATE-L model is invalidated by the data. However, that validation of the closed loop response does not imply that the model is qualified for controller design purposes.

5. SYSTEM IDENTIFIED MODEL

To complement the a priori modelling described in Section 4, we have performed system identification experiments to obtain MIMO open loop models on TCV using the method described in a companion paper [8]. Although a system identified model should also allow improved controllers to be designed, at present we have used it to validate a limited plasma open loop CREATE-L model.

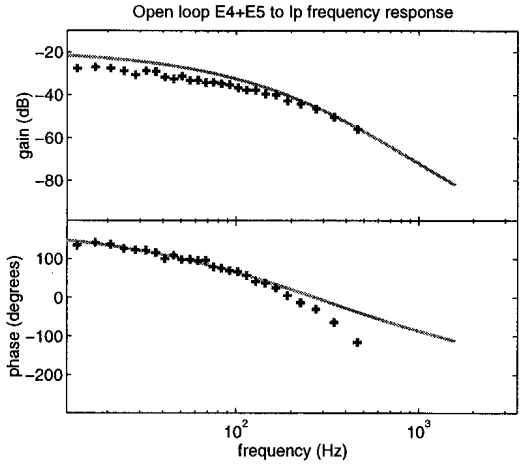

Figure 4. Comparison of CREATE-L model (solid) and system identified ('+') frequency responses for coil pair E4+E5 to plasma current.

A test signal comprising 31 frequencies was injected into the control loop, stimulating pairs of poloidal field coils with the signs chosen to stimulate only the plasma vertical position. Eight such experiments were performed, a different coil-pair stimulated in each experiment. During the experiments measurements were taken of the control voltages on the poloidal field coils and the plasma vertical position. The data collected from all the experiments was used to obtain a linear model relating the output variables to voltages on the PF coils. This approach closely follows the RBS excitation of the individual coil pairs, described in Section 4, and was chosen to identify the most critical parameters of the open loop system, namely its open loop growth rate and the relative responses of the individual coil pairs.

Some of the coils provoke a strong response of the vertical position and their transfer functions are identifiable. Other coil pairs have a small high frequency response and the analysis is limited by intrinsic noise in the tokamak plant. The output of the thyristor power supplies has a sawtooth "noise" which interferes with the analysis of the data. The amplitude of the applied stimulation is limited by mechanical stressing of the device and the time of the stimulation is limited by the duration of the quasi-stationary period of the plasma discharge. The results obtained were compared with the CREATE-L model and were found to be within good agreement.

A further series of eight experiments was performed to excite shape responses other than vertical position and the plasma current. Different output parameters were examined including combinations of various flux loops and the results found to be in general agreement with the model, as in for example Fig. 4.

6. TCV MIMO CONTROLLER PERFORMANCE

One of the MIMO controllers (PCG) used for TCV is designed around the following logical steps:

- Close the vertical position loop with an empirically tuned PID controller. The remaining plant is now stable.
- Approximate the plasma current as an inductor which has a fixed mutual inductance to all control coils.
- Calculate the DC response of the magnetic control variables to changes in the coil currents.
- Invert this sensitivity matrix, providing approximate low frequency current changes to correct the errors in the control parameters.
- Define time constants for restoring the errors in order to fix the proportional gains, and the time constants for relative integral and derivative action.
- The derived current change rates are multiplied by the DC mutual inductance matrix to obtain correction voltages.

Pulse changes in the control variable reference signals demonstrate that this approach can give some decoupling and can be used for tuning the time constants in the controller. However, the same tests show that for a diverted plasma this decoupling is quite poor (Fig. 5). Particularly bad is the coupling between plasma vertical position reference changes and the field curvature variables.

Taking the DC sensitivity matrix and the DC mutual inductance matrix, and ignoring the plasma, leaves all of the plasma response as a parasitic effect. When making rapid changes to the reference inputs to the controller, problems occur during the transient, assumedly as a result of having neglected the passive structure currents. These two shortcomings alone justify searching for methods of improving the controller. Although for the work on ITER, the design has the requirement of reducing the voltages resulting from feedback actions, for TCV this is not the case since we have a wide voltage margin and a large power surge capability.

The motivation of the modelling is to design controllers with superior performance to that currently used and to test that such performance is achievable given the plant uncertainties inherent in tokamaks. The $\mathbf{H}_\infty$ controller design method has been proposed for ITER [9]

and an appropriate design has been developed for TCV. This was done using a reduced-order plasma model, and was designed to reduce the control parameter errors when tracking reference signals. The error was filtered by appropriate weighting functions. Weights were also used to penalize the amplitude of the coil voltages and currents. The controller robustness properties were included by considering unstructured uncertainties in the plasma model. The resulting continuous time controller was reduced in order and then converted to discrete time using the Tustin bilinear approximation.

The simulated result in Fig. 5 shows the controller performance is greatly improved in comparison to the PID for a field curvature control variable. Such a design will be tested on the tokamak, along with PID controllers tuned with the model for both the scalar vertical position loop and the MIMO loop.

7. SUMMARY

We have demonstrated the performance improvements available given improved models and high order controllers on a SISO COMPASS-D loop. Work on MIMO modelling and control of TCV has also been presented. An a priori physics based model has been validated with closed loop experiments. To complement the a priori model we have also presented a MIMO system identified model of the tokamak. These models allow the design of controllers to be assessed and improved. As well as examining their performance on the TCV tokamak, we will consider the ability of the different controllers to control the different models

The potential benefits of these models are great and is demonstrated by the decoupling performance of an existing TCV controller and an $\mathbf{H}_\infty$ design. The improvement offered motivates a programme of experiments to systematically improve the controller. When judging the performance of the model-designed controllers, we will assess whether the models used are adequate to enhance the performance of the TCV control loop or whether unpredicted or neglected effects occur which destroy the nominal enhanced performance. However, given these provisos we can be confident that the answer to the question "can we enhance the performance of a tokamak using a higher order controller" is affirmative.

ACKNOWLEDGEMENTS

It is a pleasure to acknowledge Prof. Guglielmo Rubinacci of the CREATE team for stimulating discussions and also the technical support of the TCV team. Encouragement by the Naka ITER JCT is welcomed. This work was partly supported by a EURATOM mobility contract and partly by the Fonds national suisse de la recherche scientifique.

The work on COMPASS-D was carried out with the enthusiastic support of William Morris at UKAEA Fusion, Culham, UK, and with the help of useful discussions with Dr Denis Mustafa and Dr. Basil Kouvaritakis, University of Oxford, UK. It was jointly funded by the UK Department of Trade and Industry and EURATOM, with financial support from the UK Engineering and Physical Sciences Research Council.

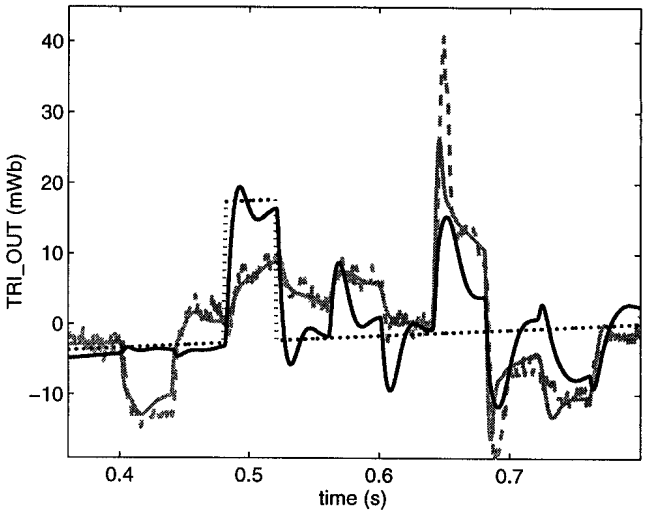

Figure 5. Comparison of decoupling performance for experimental outboard field curvature signal (dashed) and simulated results with the PID (light solid) controller and an H_∞ controller (dark solid). A pulse reference signal (dotted) is applied to each control variable in turn during the discharge.

REFERENCES

[1] P. Vyas, "Plasma Vertical Position Control in the COMPASS-D Tokamak," D.Phil. thesis, Dept. of Engineering Science, University of Oxford (1996)

[2] P. Vyas, D. Mustafa, and A. W. Morris, "Vertical Position Control on COMPASS-D," submitted to *Fusion Technology* (1997)

[3] J.R. Gossner, P. Vyas, B. Kouvaritakis, "Application of Cautious Stable Predictive Control to Vertical Positioning in COMPASS-D Tokamak," Oxford University Tech. Report, OUEL 2092/96, submitted to *IEEE Trans. on Control Systems* (1996)

[4] J.B. Lister, et al., "The Control of TCV Plasmas," EPF Lausanne Report LRP 518/95, accepted for publication in *Fusion Technology* (1996)

[5] R. Albanese and F. Villone, "The Linearized CREATE-L Model Plasma Response Model for the Control of Current, Position and Shape in Tokamaks," submitted to *Nuclear Fusion* (1997)

[6] F. Villone, et al., "Comparison of the CREATE-L Plasma Response Model with TCV Limited Discharges," EPF Lausanne Report LRP 569/97, accepted for publication in *Nuclear Fusion* (1997)

[7] P. Vyas, et al., "The Separatrix Response of Diverted TCV Plasmas Compared to the CREATE-L Model," EPF Lausanne Report LRP 583/97 (1997)

[8] A. Coutlis, et al., "An H^∞ System Identification Algorithm Applied to Tokamak Modelling," this session (1997)

[9] G. Ambrosino, et al., "Plasma Current and Shape Control in Tokamaks using H_∞ and μ-synthesis", this session (1997)

An $\mathcal{H}^\infty$ System Identification Algorithm Applied to Tokamak Modelling

A. Coutlis, D.J.N. Limebeer and J. Wainwright,
Centre for Process Systems Eng. and Dept. of Electrical Eng.,
Imperial College, London SW7 2BY, United Kingdom.
Email: a.coutlis@ic.ac.uk, d.limebeer@ic.ac.uk and j.wainwright@ic.ac.uk

J.B. Lister, P. Vyas and D.J. Ward
Centre de Recherches en Physique de Plasmas,
École Polytechnique Fédérale de Lausanne, 1015 Lausanne, Switzerland.
Email: lister@eltca1.epfl.ch, vyas@crppsun4.epfl.ch and ward@crppsun3.epfl.ch

Abstract

In this paper we describe the application of MISO System Identification to Tokamak simulations and machines. The work is motivated by the desire to create linear models for the design of modern controllers. The method described in this paper is a worst-case identification technique, in that it aims to minimise the $\mathcal{H}^\infty$ error between the identified model and the plant. Such a model is particularly suited for robust controller design. The method is fully detailed from the design of identification experiments through to the creation of a low-order model from a combination of Hankel model reduction and Chebycheff approximation. We show results from the application of this method to a powerful Tokamak Simulation Code (TSC) and discuss results on the TCV Tokamak in Lausanne.

1 Introduction

The next step in Tokamak development will be the International Thermonuclear Experimental Reactor (ITER). This machine is currently being designed and because it will be significantly different to present machines, its behaviour is simulated using a powerful non-linear Tokamak Simulation Code (TSC). However it is appropriate to use linearised models of the Tokamak system for control design and for examining general properties of the system. Linear models simulating ITER may be obtained from the local linearisation of a reduced physics non-linear simulation [1] and this method is producing useful results (see companion paper by Lister *et al.*). However this method cannot be applied to the full tokamak simulation. System identification will be able to generate a unique linear model of the most realistic simulated plasma. This model may be used to verify other linear models and will be particularly suited for the design of robust controllers. The techniques developed from work on TSC are also being applied to the TCV Tokamak in Lausanne and if the work is successful it will be an invaluable tool.

In this paper we present an $\mathcal{H}^\infty$ system identification technique to be used for the identification of linear models of TSC and TCV. The main characteristics of the linear models we identify are that they are continuous-time, MISO and unstable. The method is based on the two-stage identification algorithms presented in [7, 8, 6]. The first stage, discussed in Section 2, consists of designing multi-sinusoidal experiments for the closed-loop system, using the bilinear formula to select the measurement frequencies. We then use least-squares approximation as a generalised DFT for obtaining the frequency response estimates. In the second stage (Section 3), non-linear algorithms are used for the identification of a high-order non-causal FIR model. Finally, Hankel model reduction and MISO Chebycheff approximation methods are employed to obtain the low-order IIR identified model [4, 3]. (A survey of different identification techniques is presented in [10, 11]). Results from the application of the identification algorithm on TSC, and from the identification experiments on TCV are shown in Section 4.

2 Frequency Response Estimation

2.1 Experiment Design

A test-signal is designed, to drive the reference input of the closed-loop system during the identification experiment. The test-signal $s(t)$ is a sum of sine waves,

$$s(t) = \sum_{i=0}^{N} A_i \cos(\omega_i t + \phi_i) \ ,$$

with

$$\omega_i = w_o \tan\left(\frac{\pi i}{2L}\right) \ , \quad i = 1, \ldots, N \ , \quad N < L \ .$$

The warping formula used to select the measurement frequencies, ω_i, is the same as the one used in [8]. Both w_o and L are used to position the measurement frequencies. They must be chosen so that the measurement frequencies cover the important range of the systems response. Additional frequencies can be designed into the signal, for example around the closed-loop bandwidth.

An estimate of the dc gain of the system is also required. It can be obtained by a dc bias in the test signal, i.e. $\omega_0 = 0$, or if this is not possible, by choosing ω_0 small enough.

During the identification experiment, measurements of the input and the output of the open-loop system are taken over a time interval which is longer than the period of the lowest-frequency sinusoid. Note, that measurements must be taken after transients have died out and that the sampling frequency must be well over the Nyquist frequency, $\omega_N/2$.

Experiments equal to the number of inputs to the system are performed. These experiments must be independent, a notion defined in Section 2.3. As an example, if the test-signal is applied to a different input in each experiment while all other inputs are set to zero then, the experiments are independent.

2.2 Curve Fitting

Assuming that the system is LTI and ignoring the effect of noise and external disturbances, the frequency content of the measured signals will lie on the measurement frequencies designed into the test-signal. The frequency spectrum of the measured signals at these frequencies is obtained by least squares approximation.

We choose sines and cosines of the measurement frequencies (ω_i) as basis functions and define the approximation error,

$$e_k = u(kt_s) - \sum_{i=0}^{N} B_i \cos(\omega_i k t_s) + C_i \sin(\omega_i k t_s) \ ,$$

where $u(kt_s)$ is the measured signal and t_s the sampling time. We compute B_i and C_i ($C_0 = 0$ if $\omega_0 = 0$) such that the square of the error $e^T e$, is minimised, where e is the vector of errors,

$$e = [e_0 \ e_2 \ \cdots \ e_k \ \cdots \ e_m]^T \ .$$

Then, the frequency component of the measured signal at ω_i is defined as $A_i e^{j\phi_i}$, where

$$A_i = \sqrt{B_i^2 + C_i^2} \ \ and \ \ \phi_i = \tan^{-1}(-C_i/B_i) \ .$$

The amplitudes of the residuals e_i, which cannot be decomposed into the measurement frequencies are a measure of the external disturbances, non-linearities of the system and measurement noise. Therefore, the smaller the residuals compared to the measured signals the greater the confidence in the results of the identification procedure.

2.3 Frequency Response Estimation

Using the technique above, the frequency spectra of all input and output data collected during the identification experiments is estimated. Hence, for a MISO $1 \times q$ system we obtain, $U_k^j(\omega_i)$, the frequency spectrum at ω_i of the k-th input from the j-th experiment for, $i = 0, \ldots, N$, $k = 1, \ldots, q$ and $j = 1, \ldots, q$ and $Y^j(\omega_i)$ the frequency spectrum at ω_i of the output from the j-th experiment for, $i = 0, \ldots, N$ and $j = 1, \ldots, q$. By considering all experiments we have,

$$\hat{G}(\omega_i) = \begin{bmatrix} Y^1(\omega_i) \\ \vdots \\ Y^q(\omega_i) \end{bmatrix}^T \begin{bmatrix} U_1^1(\omega_i) & \cdots & U_1^q(\omega_i) \\ \vdots & & \vdots \\ U_q^1(\omega_i) & \cdots & U_q^q(\omega_i) \end{bmatrix}^{-1} \ ,$$

for all $i = 0, \ldots, N$. Hence we obtain frequency response estimates of the system at the measurement frequencies, $\omega_0, \ldots, \omega_N$. The invertibility of the U matrix is a mild condition which is satisfied if the corresponding matrix for the designed test-signal is invertible. If that is the case, then the experiments performed are said to be independent.

3 Transfer Function Identification

3.1 FIR Model Estimation

We have obtained frequency response estimates on frequencies given by, $\omega_i = w_o \tan(\pi i/2L)$. Given that we can map the continuous-time system $G(s)$ into discrete-time via the bilinear transformation

$$G^d(z) = G(s)|_{s = w_o \frac{z-1}{z+1}}$$

we have that on the measurement frequencies,

$$G^d\left(e^{\frac{i\pi i}{L}}\right) = G(\omega_i) \ ,$$

for $i = 0, \ldots, N$. Hence we have obtained frequency response estimates of G^d at equispaced frequencies on the unit circle.

From an IDFT on the frequency response estimates we obtain an estimate of the impulse response of $G^d(z)$,

$$\hat{g}_k = \frac{1}{2L} \sum_{i=-N}^{N} \hat{G}(\omega_i) e^{jk\pi i/L} \ .$$

Now we relate this estimate of the impulse response coefficients to the true coefficients of the equivalent under the bilinear transformation discrete-time system, $G^d(z)$. From the definition of a discrete-time system

$$\begin{aligned} G^d(e^{j\pi i/L}) &= \sum_{k=-\infty}^{\infty} g_k e^{-j\pi ki/L} \\ &= \sum_{k=0}^{2L-1} \sum_{l=-\infty}^{\infty} g_{k+2lL} e^{-j\pi ki/L} , \end{aligned}$$

hence,

$$\hat{g}_k = g_k + \sum_{l=-\infty,\ l\neq 0}^{\infty} g_{k+2lL} ,$$

if $L = N + 1$ and $G(\infty) = G^d(-1) = 0$.

If we have chosen L greater than the impulse response length of the causal and anticausal parts of $G^d(z)$ system i.e. $L > IRL_s$ and $L > IRL_u$, then

$$\hat{g}_k \approx \begin{cases} g_k, & for\ 1 \leq k \leq L \\ g_{k-2L}, & for\ L+1 \leq k \leq 2L \end{cases} ,$$

where $\hat{g}_{2L} = \hat{g}_0$. Hence $\hat{g}_k$ for $1 \leq k \leq L$ approximates the causal part of $G^d(z)$ and $\hat{g}_k$ for $L + 1 \leq k \leq 2L$ is diverging, approximating the anticausal part shifted by $2L$. The impulse response lengths of the causal and anticausal part of the system need not be the same. If for example, the length of the anticausal response is shorter than that of the causal impulse response then fewer than L elements, at the tail of $\hat{g}_k$ will represent the anticausal part, while more than L elements in the beginning of $\hat{g}_k$ will represent the causal part. In general, the converging part of the $\hat{g}_k$ sequence is dominated by the causal part and the diverging, if it exists, by the anti-causal part. A minimum requirement for N is to be larger than the sum of the causal and anticausal impulse response lengths, $IRL_u + IRL_s$.

Once the impulse response coefficients $\hat{g}_k$, $k = 0, \ldots, 2L-1$ have been identified from the frequency response estimates of the system, two pre-identified models are constructed one for the stable and one for the antistable part,

$$\hat{G}^{d,st}_{p-id} = \sum_{k=1}^{m_s} a^{st}_k \hat{g}_k z^{-k}$$

and

$$\hat{G}^{d,ast}_{p-id} = \sum_{k=0}^{-m_u} a^{ast}_k \hat{g}_{2L+k} z^{-k} .$$

where $m_s + m_u < 2L$, and a^{st}_k, a^{ast}_k are given window functions [6, 2]. The variables m_s and m_u are chosen to approximate the impulse response lengths of the stable and antistable part of the system respectively, which in turn are estimated from the identified $\hat{g}_k$ sequence. The variable m_s is chosen to be the length of the converging part and m_u the length of the diverging part of the $\hat{g}_k$ sequence.

The inverse bilinear transformation is employed to obtain the continuous-time FIR model of the system from the discrete-time FIR model. The transformation is,

$$\hat{G}_{p-id}(s) = \hat{G}^d_{p-id}(z)\big|_{\ z=(w_o+s)/(w_o-s)} .$$

Thus the pre-identified state-space model of the continuous-time system $\hat{G}_{p-id} \stackrel{s}{=} (\hat{A},\ \hat{B},\ \hat{C},\ \hat{D})$ is given from the state space model of $\hat{G}^d_{p-id}(z)$,

$$\hat{G}^d_{p-id}(z) = \hat{G}^{d,st}_{p-id}(z) + \hat{G}^{d,ast}_{p-id}(z) \stackrel{s}{=} (\hat{A}^d,\ \hat{B}^d,\ \hat{C}^d,\ \hat{D}^d)$$

from

$$\begin{aligned} \hat{D} &= \hat{D}^d - \hat{C}^d(I + \hat{A}^d)^{-1}\hat{B}^d , \\ \hat{C} &= \sqrt{2w_o}\hat{C}^d(I + \hat{A}^d)^{-1} , \\ \hat{B} &= \sqrt{2w_o}(I + \hat{A}^d)^{-1}\hat{B}^d , \\ \hat{A} &= w_o(\hat{A}^d - I)(I + \hat{A}^d)^{-1} . \end{aligned}$$

3.2 Order Selection

The hankel singular values (h.s.v.'s) of the pre-identified state-space model are used to estimate the order of the low-order model which describes the plant. We know that the infinity norm of the error between an mth order stable model $\hat{G}$ and an rth order Hankel approximation $\tilde{G}_H$ (stable) is bounded by,

$$\sigma_{r+1} \leq \left| \hat{G} - \tilde{G}_H \right|_\infty \leq \sum_{i=r+1}^{m} \sigma_i$$

where the σ_i's represent the h.s.v.'s values of $\hat{G}$ ordered in decreasing order of magnitude. Note, that the lower bound is valid for any stable rth order approximation. Looking at the σ_i's we can choose an order for the low-order approximation and use Hankel model reduction to obtain the stable model [5], $\tilde{G}_H \stackrel{s}{=} (\tilde{A}_H,\ \tilde{B}_H,\ \tilde{C}_H, \tilde{D}_H)$. For weighted Hankel model reduction refer to [5].

The stable and unstable projections of the pre-identified model are treated separately. The stable projection, $\hat{G}^{st}_{p-id}$ is model reduced directly and yields, $\tilde{G}^{st}_H$. For the unstable part we model reduce its para-hermitian conjugate $(\hat{G}^{ast}_{p-id})^\sim$, which is stable, to obtain the stable approximation $(\tilde{G}^{ast}_H)^\sim$. Then, $\tilde{G}^{ast}_H$ is the reduced-order model for $\hat{G}^{ast}_{p-id}$ and the complete Hankel model is,

$$\tilde{G}_H = \tilde{G}^{st}_H + \tilde{G}^{ast}_H \stackrel{s}{=} (\tilde{A}_H,\ \tilde{B}_H,\ \tilde{C}_H, \tilde{D}_H) .$$

3.3 The Identified Model

To obtain the final identified model we use Chebycheff approximation. The method for MIMO systems can be found in [4]. Here we concentrate on the MISO case.

In one approach, the "zero-only" tuning algorithm, we consider tuning the zero polynomial of the identified model $\tilde{G}_I(s)$, such that,

$$\tilde{G}_I(s) = \arg\min_{\tilde{G}(s)} \max_{s_i=j\omega_i} \left| \left(\hat{G}(s_i) - \tilde{G}(s_i)\right) W(s_i) \right| \quad (1)$$

with the pole polynomial given from the rth order Hankel model, that is

$$\tilde{G}_I(s) = \frac{\tilde{N}_I(s)}{\tilde{d}_H(s)} = \frac{\sum_{l=0}^{n} \mathbf{b_l}^T s^l}{\tilde{d}_H(s)}, \qquad n \leq r \ .$$

where $W(s)$ is a given weighting function and $\mathbf{b_l}$ are q-dimensional column vectors.

The zero-only approximation problem (1) is solved with respect to the $\mathbf{b_l}$'s, by the following minimax problem,

$$\begin{aligned} &\textit{minimise} && \epsilon \\ &\textit{subject to} && \epsilon + \Re\left\{ \frac{\sum_{l=0}^{n} \mathbf{b_l}^T s_i^l}{\tilde{d}_H(s_i)} W(s_i)\mathbf{v^i} \right\} \\ & && \geq \Re\left\{ \hat{G}(s_i) W(s_i) \mathbf{v^i} \right\} \end{aligned}$$

for all $i = 0, \ldots, N-1$ and all $|\mathbf{v^i}| = 1$ with $\epsilon > 0$. This minimax problem is solved as a linear program by writing it into the equivalent form,

$$\begin{aligned} &\textit{minimise} && \epsilon \\ &\textit{subject to} && \begin{bmatrix} \mathbf{b_0} \\ \vdots \\ \mathbf{b_n} \\ \epsilon \end{bmatrix}^T \Re\left\{ \begin{bmatrix} W(s_i)\mathbf{v^i} \\ \vdots \\ W(s_i)\mathbf{v^i} s_i^n \\ 1 \end{bmatrix} \right\} \\ & && \geq \Re\left\{ \hat{G}(s_i) W(s_i) \mathbf{v^i} \right\} \ . \quad (2) \end{aligned}$$

This is a convex problem and the solution found is guaranteed to be optimal [2, Characterisation theorem]. The algorithm solving the linear program (2) can also be found in [2].

It is also possible to use an $\mathcal{L}^\infty$ variant of Levy's method [9, 4] to tune both the poles and the zeros of the SIMO identified model $\tilde{G}_I(s)$. This is the "zero-and-pole" identification problem: find $\mathbf{b_l}$, $l = 0, \ldots, n$ and a_k, $k = 1, \ldots, r$ such that

$$\tilde{G}_I(s) = \frac{\tilde{N}_I(s)}{1 + \tilde{\phi}_I(s)} = \frac{\sum_{l=0}^{n} \mathbf{b_l}^T s^l}{1 + \sum_{k=1}^{r} a_k s^k}, \qquad n \leq r+1$$

minimises the infinity-norm of the identification error,

$$\tilde{G}_I = \min_{\tilde{N}_I,\ \tilde{\phi}_I} \max_{i=0,\ldots,N-1} \left| \left(\hat{G}(s_i) - \tilde{G}_I(s_i)\right) W(s_i) \right| . \quad (3)$$

This approximation problem is solved by an iterative process:

$$\tilde{N}_I^{m+1},\ \tilde{\phi}_I^{m+1} =$$

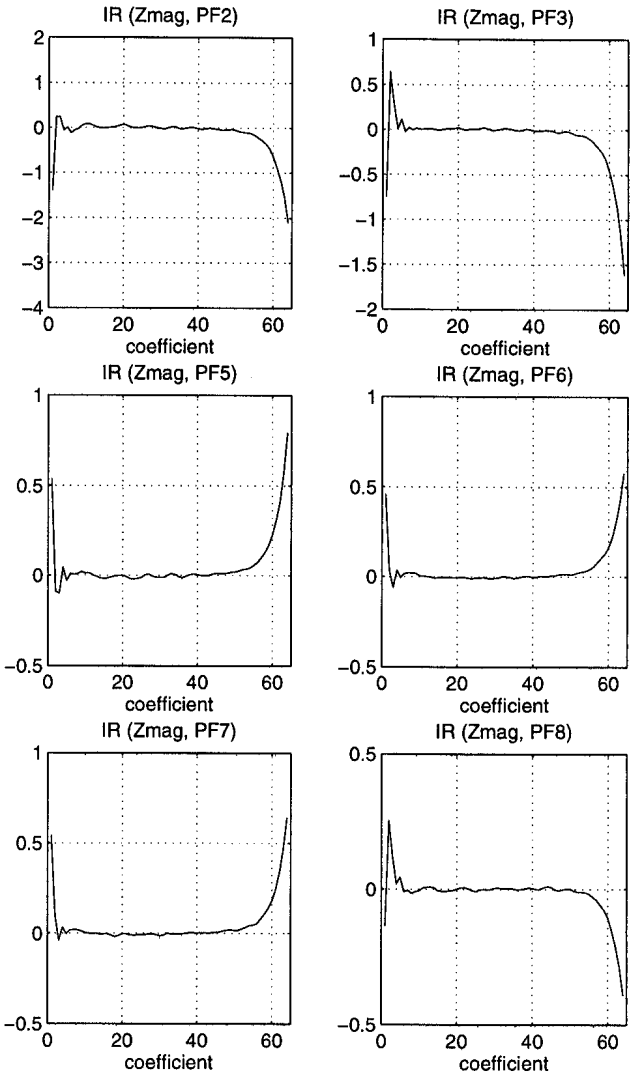

Figure 1: Estimated impulse response of Z_m vs V_{PF2}, V_{PF3} and V_{PF5} to V_{PF8} subsystems of G^d.

$$\arg\min_{N,\phi} \max_{i} \left| \left[\hat{G}(s_i)\left(1 + \phi(s_i)\right) - N(s_i)\right] w^m(s_i) \right| , \quad (4)$$

where in each iteration $m = 1, 2, \ldots$ we update $w^m(s) = W(s_i)/(1 + \tilde{\phi}_I^m(s))$ with $w^1(s) = W(s_i)/(1 + \hat{\phi}^H(s))$ and $\hat{\phi}^H(s)$ given from $\tilde{G}_H(s)$. Once this process has converged, after M iterations say, the resulting model is given by

$$\tilde{G}_I(s) = \frac{\tilde{N}_I(s)}{1 + \tilde{\phi}_I(s)} = \frac{\tilde{N}_I^M(s)}{1 + \tilde{\phi}_I^M(s)}.$$

The linear program which solves the mth iteration is,

$$\begin{aligned} &\textit{minimise} && \epsilon \\ &\textit{subject to} \end{aligned}$$

$$\begin{bmatrix} \mathbf{b_0} \\ \vdots \\ \mathbf{b_n} \\ -a_1 \\ \vdots \\ -a_r \\ \epsilon \end{bmatrix}^T \Re\left\{ \begin{bmatrix} w^m(s_i)\mathbf{v^i} \\ \vdots \\ w^m(s_i)\mathbf{v^i}s_i^n \\ \hat{G}(s_i)w^m(s_i)\mathbf{v^i} \begin{bmatrix} s_i \\ \vdots \\ s_i^r \end{bmatrix} \\ 1 \end{bmatrix} \right\}$$

$$\geq \Re\left\{\hat{G}(s_i)w^m(s_i)\mathbf{v^i}\right\} . \qquad (5)$$

The zero-and-pole approximation problem is non-convex and the iterations (4) need not converge. However, if they converge then the solution of (5) is the global optimum of the zero-and-pole approximation problem (3), [2].

Furthermore, it has to be checked a posteriori whether the identified model obtained from zero-and-pole tuning has a number of unstable poles compatible with the Hankel singular values of the FIR model ([2]).

4 Tokamak Identification

4.1 TSC Results

The purpose of this case study is to identify a linear model for TSC. The simulations assumed an artificially large plasma mass in order to speed-up the run-time. A transfer function model is required to relate the vertical displacement of the plasma magnetic axis Z_m, to the voltages on the poloidal field coils V_{PF2}, V_{PF3} and V_{PF5} to V_{PF8}.

The test signal is a sinusoid with 31 frequencies,

$$\sum_{i=1}^{31} 1kV \ \cos(\omega_i t + \phi_i)$$

with

$$\omega_i = 2\tan\left(\frac{i\pi}{64}\right) .$$

The measurement frequencies span the range $\omega_1 = 0.098 rad/s$ to $\omega_{31} = 40 rad/s$. The test signal is designed for application to each coil in turn, each simulation being an identification experiment. In total 6 identification experiments (IDEs) were performed.

Available experiment time is $140s$. Allowing $20s$ for transients to die out that leaves $120s$ of measurements available for the identification algorithm. The period of the slowest sinewave ($2\pi/\omega_1 = 64s$) was designed to be well below $120s$. Similarly the highest frequency was designed to be well above the sampling frequency which was $155 rad/s$, in line with experiment design restrictions (Section 2.1).

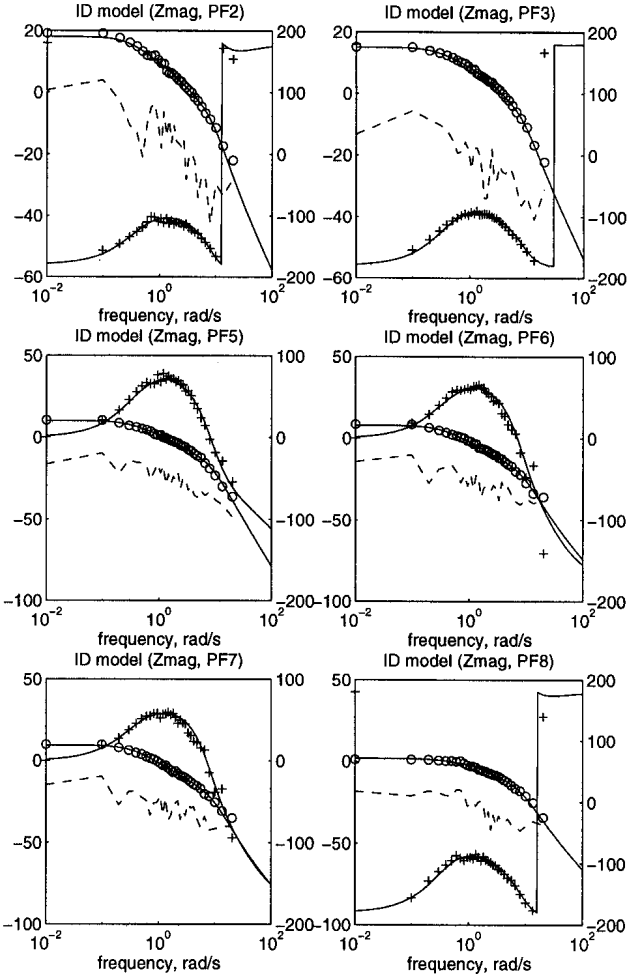

Figure 2: Final Chebycheff identified model (solid), frequency response estimates (amplitudes-circles, phases-crosses) and error with respect to the frequency response estimates (dashed). Amplitude axis in dB on the left, phase axis in degrees on the right.

From the frequency response estimates obtained from the measured input and output sequences (Sections 2.2 and 2.3) a pole well below the lowest measurement frequency was identified. This is in fact a pole at the origin due to the superconducting coils. The effect of this pole was removed in the subsequent calculations by multiplying the frequency response estimates $\hat{G}(j\omega_i)$ by $j\omega_i$. An estimate for the dc gain of the system was given from $sign\left(\hat{G}(j\omega_1)\right)|\hat{G}(j\omega_1)|$.

From the frequency response estimates the impulse response of the discrete-time equivalent system G^d is estimated (Fig. 1), as described in Section 3.1. The length of the stable part, the converging part of the impulse response in Fig. 1 is chosen as 15. The length of the antistable part, the diverging part of the impulse response in Fig. 1 is chosen as 26, that is starting from coeffi-

cient 38 (Section 3.1). No windowing function is used for the calculation of the pre-identified model $\hat{G}^d_{p-id}$ (i.e. $a^{st}_k = 1$ and $a^{ast}_k = 1$ for all k) since the noise level in the measured signals estimated from the residuals (Section 2.2) was very small.

The zero-and-pole Chebycheff algorithm (Section 3.3) is used to obtain the final identified model. The error on each frequency response estimate is weighted by the inverse amplitude of the frequency response estimate. This weighting is up to the frequency $8rad/s$ above which, the weight amplitude remains constant. The weight on the error for the subsystem corresponding to PF8 is increased by a factor of 2. A 4th order model is obtained shown in Fig. 2. The value of the unstable pole of the system has been identified to be $0.32rad/s$. This value has been verified in subsequent open-loop simulations.

4.2 TCV Experiments

The same identification techniques have been used to identify linear models for a real tokamak machine, the TCV. The test-signal for the TCV experiment comprised of 29 sinewaves, the measurement frequencies chosen as,

$$\omega_i = 430 \tan\left(\frac{i\pi}{64}\right) , \qquad i = 1, \ldots 29 .$$

A total of 8 identification experiments were run each stimulating a different coil pair. The aim is to identify a linear model relating the product of the plasma current and the displacement of the magnetic axis $Z_m I_p$ to the voltage on the 8 poloidal coil-pairs driven in anti-symmetric mode.

The results obtained compared very well with existing physical models, proving the application of the technique to real systems as well as non-linear simulation code.

5 Summary

We have presented an $\mathcal{H}^\infty$ identification technique for MISO, unstable and continuous-time systems. The technique has successfully identified a linear model for TSC. It has also been shown by experiments on TCV that the same technique developed for TSC can be applied successfully to a real tokamak machine.

References

[1] R. Albanese, E. Coccorese, and G Rubinacci. *Nuclear Fusion*, 29(6):1013, 1989.

[2] A. Coutlis. *System Identification for MIMO Discrete and Continuous-Time Systems.* PhD thesis, Department of Electrical and Electronic Eng., Imperial College, London, UK, March 1997.

[3] A. Coutlis and D.J.N. Limebeer. Control oriented system identification for MIMO continuous and discrete-time systems. *Proc. 35th Conf. on Decision and Control*, 1996. Kobe, JAPAN.

[4] A. Coutlis and D.J.N. Limebeer. Chebycheff approximation in system identification and model reduction. *Automatica*, 32, 1997.

[5] M. Green and D.J.N. Limebeer. *Linear Robust Control.* Prentice Hall, 1995.

[6] G. Gu and P.P. Khargonekar. Linear and nonlinear algorithms for identification in $\mathcal{H}^\infty$ with error bounds. *IEEE Trans. Autom. Control*, 37:953–963, 1992.

[7] A.J. Helmicki, C.A. Jacobson, and C.N. Nett. Control oriented system identification: A worst-case deterministic approach in $\mathcal{H}^\infty$. *IEEE Trans. Autom. Control*, 36:1163–1176, 1991.

[8] A.J. Helmicki, C.A. Jacobson, and C.N. Nett. Worst-case deterministic identification in $\mathcal{H}^\infty$: The continuous-time case. *IEEE Trans. Autom. Control*, 37:604–610, 1992.

[9] E.C. Levy. Complex curve fitting. *IRE Trans. Autom. Control*, pages 37–43, 1959.

[10] P.M. Mäkilä, J.R. Partington, and T.K. Gustafsson. Worst-case control-relevant identification. *Automatica*, 31:1799–1819, 1995.

[11] B. Ninness and G.C. Goodwin. Estimation of model quality. *Automatica*, 31:1771–1797, 1995.